relationship among the modes should be, since it is not possible to meet the simple unambiguous criterion that the negative absorption of all modes shall be maximum simultaneously. This question is still under study.

ACKNOWLEDGMENT

We thank R. A. Paananen for contributions to this work. We should like also to thank Professor N. Bloembergen and Professor P. Pershan for a helpful discussion.

PHYSICAL REVIEW VOLUME 128, NUMBER 3 NOVEMBER 1, 1962

Magnetoacoustic Measurements in the Noble Metals at 350 Mc/sec*

HENRY V. BOHM AND VERNON J. EASTERLING
Department of Physics, Wayne State University, Detroit, Michigan
(Received May 28, 1962)

Further magnetoacoustic measurements on the noble metals are presented for frequencies up to 350 Mc/sec. Plots of the ultrasonic pulse height, h, vs the reciprocal of the magnetic field strength, $1/H$, show 20 or more maxima and minima for several orientations in each metal. Fermi surface dimensions are calculated from the periods in $1/H$ of the magnetoacoustic oscillations using the interpretation that the periodicity arises from those portions of the Fermi surface which are extremal in the $\mathbf{q}\times\mathbf{H}$ direction of momentum space; Fermi surface cross sections viewed along the [100], [110], [111], and [112] directions are shown in detail. The results are compared with Fermi surface dimensions given by: (1) other magnetoacoustic effect data, (2) de Haas-van Alphen and anomalous skin-effect data, and (3) recent band theory calculations. Some simple calculations of electron mean free paths and collision relaxation times are given.

INTRODUCTION

In this paper we shall present further noble metals Fermi surface dimensions[1–6] derived from magnetoacoustic-effect data. The oscillatory variation of ultrasonic attenuation as a function of magnetic field intensity (magnetoacoustic effect) occurs only in very pure metals at low temperatures due to the requirement that the electronic mean free path be much greater than the sound wavelength, λ. The oscillations which are periodic in H^{-1} (H is the magnetic field strength) occur because of geometrical coincidences between certain electron orbits and the periodic electric fields accompanying the sound wave. The effect, when $\mathbf{H}$ is perpendicular to the sound propagation vector $\mathbf{q}$ (q is $2\pi/\lambda$), gives the dimensions and ultimately the shape of the Fermi surface if we make the interpretation that the period observed in H^{-1} is determined by the Fermi momentum perpendicular to $\mathbf{H}$ and $\mathbf{q}$ at those portions of the surface where this momentum is extremal.[7–10] If $\hbar k$ is such a momentum and $\Delta(H^{-1})$ is the corresponding magnetoacoustic period, then

$$\hbar k=(e\lambda/2c)[1/\Delta(1/H)]. \quad (1)$$

Almost all data were taken using longitudinal sound waves, the sound propagation directions studied being [100], [110], and [111] for all three metals, and additionally [112] in gold and copper. In these experiments the magnetic field can be given any direction in a plane perpendicular to $\mathbf{q}$. The longitudinal velocities, lattice constants, and free-electron sphere radii for the noble metals are given in Table I.[11,12] The experimental techniques and preparation of samples were essentially the same as those discussed in an earlier article[5] except that we now have equipment, constructed in our laboratory, which increases our frequency range to 350 Mc/sec. All three metals were of nominal purity 99.999% or better.

The method of plotting and analyzing the data was the same as described earlier.[5] The extremal Fermi surface dimensions corresponding to the observed periods of oscillation are interpreted in terms of the Fermi surface model shown in the extended zone scheme in Fig. 1. Some of the extremal orbits which we shall discuss are also shown in the figure.

* This research was supported by the United States Air Force through the Air Force Office of Scientific Research under contract No. AF 49(638)-832.

[1] R. W. Morse, A. Myers, and C. T. Walker, Phys. Rev. Letters 4, 605 (1960).
[2] R. W. Morse, in *The Fermi Surface*, edited by W. A. Harrison and M. B. Webb (John Wiley & Sons, Inc., New York, 1960).
[3] Reference 2, p. 245.
[4] R. W. Morse, A. Myers, and C. T. Walker, J. Acoust. Soc. Am. 33, 699 (1961).
[5] V. J. Easterling and H. V. Bohm, Phys. Rev. 125, 812 (1962).
[6] H. V. Bohm and V. J. Easterling, Bull. Am. Phys. Soc. 6, 438 (1961).
[7] M. H. Cohen, M. J. Harrison, and W. A. Harrison, Phys. Rev. 117, 937 (1960).
[8] T. Kjeldaas and T. Holstein, Phys. Rev. Letters 2, 340 (1959).
[9] A. B. Pippard, Proc. Roy. Soc. London A257, 165 (1960).
[10] V. L. Gurevitch, J. Exptl. Theoret. Phys. (U.S.S.R.) 37, 71 (1959) [translation: Soviet Physics—JETP 10, 51 (1960)].

[11] The elastic constants used in the velocity calculation are from W. C. Overton and J. Gaffney, Phys. Rev. 98, 969 (1955) for copper, and from J. R. Neighbours and G. A. Alers, Phys. Rev. 111, 707 (1958) for silver and gold.
[12] The lattice constant values at 4.2°K were calculated by taking the 25°C values given by C. S. Barrett, *Structure of Metals* (McGraw-Hill Book Company, Inc., New York, 1952), and correcting to 4.2°K using the thermal expansion data of F. C. Nix and D. McNair, Phys. Rev. 61, 74 (1942).

TABLE I. 4.2°K Longitudinal velocities, lattice constants, and free electron Fermi sphere radii.

	Longitudinal velocities (units of 10^5 cm/sec)				Lattice constants (in angstroms)	Free electron Fermi sphere radii (units of 10^{-19} g-cm/sec)
	[100]	[110]	[111]	[112]		
Cu	4.420	5.076	5.276	5.120	3.603	1.437
Ag	3.517	3.945	4.078		4.068	1.273
Au	3.217	3.444	3.516	3.453	4.065	1.274

EXPERIMENTAL RESULTS

$q \| [100]$

With $\mathbf{q} \| [110]$ and $\mathbf{H}$ maintained in a plane perpendicular to $\mathbf{q}$, the extremal momentum values observed are those given in Table II (unless otherwise specified, all dimensions are given in units of the free-electron sphere radii listed in Table I). For $\mathbf{H}$ near $[\bar{1}11]$, long-period oscillations are observed which are interpreted as being due to electrons circulating about the necks where the Fermi surface joins the (111) Brillouin zone boundary (orbit a in Fig. 1). The dependence of the period on magnetic field direction gives the shape of the neck as shown by the dots in Fig. 2. The size of the neck is largest in copper and smallest in silver; the angles subtended by the necks as they contact the Brillouin zone boundary being 20°, 14.5°, and 18.5° for copper, silver, and gold, respectively. For $\mathbf{H}$ near [001], belly oscillations are found (orbit f in Fig. 1) which measure the Fermi surface radius directly. The $\mathbf{H}$ dependence of the period gives the "belly" radii shown by the ×'s in Fig. 2. As $\mathbf{H}$ is moved away from [001], these belly oscillations disappear first in copper, then in gold, and finally in silver. This is also in order of decreasing neck size which indicates that the presence of the necks prevents central belly oscillations for a smaller angular displacement of $\mathbf{H}$ from [001] in copper, as would be expected, since the neck is largest. For $\mathbf{H}$ near $[\bar{1}10]$, two periods are observed; the longer one we interpret as being due to electrons circulating about the dog's bone orbit. Twice the momentum value is taken to be a measure of the extent of the indentation of the concave side of the dog's bone (distance A in Fig. 1). Since the electron in its trajectory moves parallel to the sound wavefronts at the corners of the dog's bone and at the center of the concave side, it seems reasonable to assume that there should be a period determined by the distance between these two points. The shorter period appears to be associated with the noncentral extremal orbit running over two necks and gives a measure of dimension B in Fig. 1. If this interpretation is correct, A plus B should be equal to the Fermi surface radius along [001]; this gives 1.100±0.060, 1.072±0.065, and 1.127±0.070 for Cu, Ag, and Au,

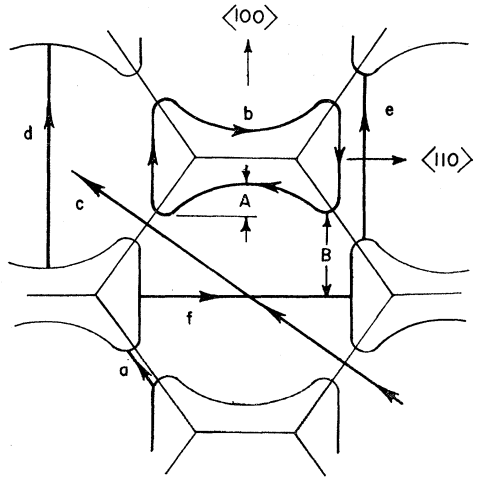

FIG. 1. Extended zone scheme showing some of the possible extremal orbits for the Fermi surface model; (a) neck orbit, (b) dog's bone, (c) open orbit, (d) and (f) central belly orbits, and (e) off-center belly orbit. All orbits except (b) are viewed edge on. The dimensions A and B are measured with $\mathbf{q} \| [110]$ as discussed in the text.

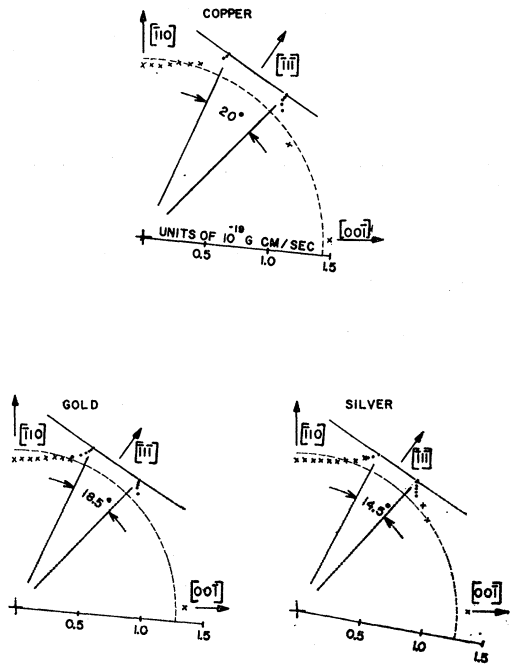

FIG. 2. Plot of experimental data in [110] Fermi surface cross section; the ×'s are belly-orbit measurements and the dots are neck-orbit measurements. The dashed lines represent a spherical Fermi surface for one free electron per atom.

TABLE II. Extremal Fermi surface dimensions for various magnetic field orientations with q parallel to [110].

H orientation	P/P_F Cu	Ag	Au
Parallel to [001]	0.956±0.011	0.955±0.012	0.933±0.011
3° from [001]	0.960±0.011	0.954±0.012	0.938±0.011
6°	0.954±0.011	0.953±0.012	0.942±0.011
9°	0.972±0.011	0.962±0.012	0.946±0.011
12°	0.990±0.011	0.974±0.012	0.958±0.012
15°	0.998±0.011	0.982±0.012	0.982±0.012
18°	1.017±0.011	1.005±0.012	0.985±0.012
21°		1.016±0.012	0.993±0.012
24°		1.062±0.012	
30°		0.208±0.017	
35°	0.244±0.014	0.193±0.015	0.236±0.008
40°	0.212±0.012	0.174±0.015	0.201±0.008
45°	0.198±0.011	0.165±0.014	0.192±0.006
		1.037±0.024	
50°	0.198±0.011	0.144±0.012	0.181±0.006
		1.037±0.024	
55° from [001] (parallel to [$\bar{1}$11])	0.195±0.011	0.142±0.012	0.180±0.006
	0.967±0.021	0.998±0.024	
60°	0.197±0.011		0.182±0.006
65°	0.204±0.011	0.173±0.015	0.189±0.006
70°		0.199±0.015	0.202±0.008
75°	0.150±0.021	0.765±0.024	0.232±0.008
		0.199±0.024	
80°	0.141±0.027	0.203±0.024	0.283±0.009
85°	0.811±0.021	0.751±0.024	0.780±0.024
	0.142±0.020	0.179±0.021	0.174±0.024
90° from [001] (parallel to [$\bar{1}$10])	0.815±0.021	0.712±0.023	0.751±0.023
	0.142±0.020	0.180±0.021	0.188±0.024

respectively. These data, some of our poorest, are in fair agreement with other measurements of the [001] radius made with $\mathbf{q}\|[100]$.

$q\|[100]$

Table III shows the data taken with the sound propagation direction along [100], where very strong oscillations are found for almost all directions of magnetic field. With **H** near [011], we observe a period which is associated with the dog's bone orbit (orbit *b* in Fig. 1). This orbit has its center of oscillation displaced by 1.809 units from the Brillouin zone center; the difference between this distance and one-half the dog's bone length gives the Fermi surface radius along [01$\bar{1}$] for each metal. As **H** is moved away from [011] by an amount greater than one-half the angle subtended by the neck, the dog's bone oscillation vanishes, and a periodicity due to a noncentral body orbit becomes dominant. In our earlier work on silver,[5] this orbit was not recognized since it has a dimension only slightly different from the central belly radius and is observed only over a 5-deg range. However, subsequent data taken on gold and more especially on copper quite clearly showed the existence of the noncentral orbit. In copper, for example, it was found that as **H** was moved from approximately 10° from [011] (where the dog's bone period must disappear) to parallel to [001], the dimension measured remains, over a 5° variation of **H**, about the same as for the dog's bone, then de-

TABLE III. Extremal Fermi surface dimensions for various magnetic field orientations with q parallel to [100].

H orientation	P/P_F Cu	Ag	Au
Parallel to [011]	0.852±0.009	0.876±0.011	0.868±0.011
3° from [011]	0.859±0.009	0.879±0.011	0.876±0.011
6°	0.871±0.009	0.886±0.011	0.889±0.011
9°	0.884±0.009	0.903±0.011	0.899±0.011
12°	0.884±0.009	0.912±0.011	0.901±0.011
15°	0.881±0.009	0.911±0.011	0.916±0.011
20°	0.874±0.018	0.919±0.011	0.927±0.011
25°	0.991±0.021	0.978±0.023	0.963±0.023
30°	0.991±0.021	0.979±0.023	1.016±0.024
35°	0.999±0.021	1.010±0.024	1.037±0.024
40°	1.020±0.021		1.052±0.026
45° from [011]; parallel to [001]	1.036±0.021		1.068±0.026

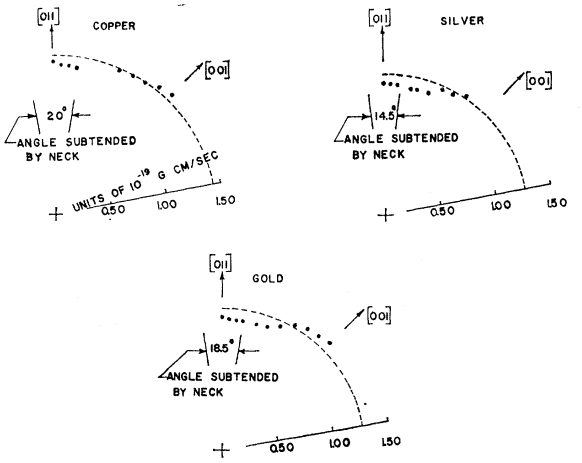

FIG. 3. Plot of experimental data in [100] Fermi surface cross section. The points within the angle subtended by the neck are dog's bone orbit data, while all other points are from belly-orbit data. The dashed lines represent free-electron sphere radii.

creases by about 2% over the next 5° interval; at **H** slightly more than 20° from [011], a beat is present at about the tenth oscillation, indicating that the observed period represents an average of two periods differing by about 10%. Two degrees further from [011], we find that the periodicity at high magnetic field is different from that below 3000 G, the low-field period giving a somewhat larger dimension. We interpret this as being a mixture of the noncentral and central orbit periods at high field, the stronger central orbit period remaining alone at low field. By moving **H** 2° further, the noncentral orbit period disappears completely, leaving only the central orbit period which we observe all the way to **H** parallel to [001]. The points plotted in Fig. 3 represent only those periods which we think are clearly from the dog's bone or central belly orbits. In silver, the oscillations become so weak for **H** within 10° of [001] that no momentum values can be obtained.

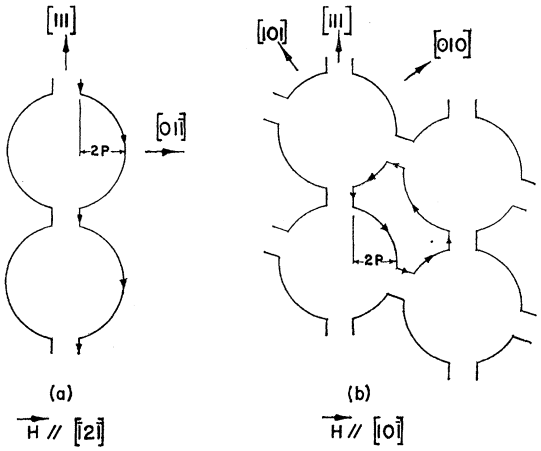

FIG. 4. Cross section of Fermi surface model showing: (a) open orbit, and (b) tilted dog's bone orbit observed with **q** along [111].

$q \| [111]$

Due to the high degree of symmetry in the (111) plane one needs to vary **H** only from [1$\bar{1}$0] to [2$\bar{1}\bar{1}$]. (We have, of course, taken data over a much wider range of **H** directions to be sure that our data properly exhibit this symmetry.) Over this entire 30-deg interval there is one dominant period which is intermediate in value between a neck and a belly period. For **H** near [2$\bar{1}\bar{1}$], the period is believed to arise from open orbits as shown in Fig. 4(a). If this interpretation is correct, then twice the measured momentum plus the neck radius should give the belly dimension of the Fermi surface along [110] directions. (Since this dimension is also measured with **q** along [110] and [100], we have a check on our interpretation and quite good agreement is found.) When **H** is near [1$\bar{1}$0], the central orbit passes through four necks and the electron path is around the "tilted dog's bone" as indicated in Fig. 4(b). However, the momentum found at this orientation in each of the metals is only about one-half of what one would expect for the dog's bone path; further, the phase of the oscillation, as determined by the n vs H^{-1} plots described in reference 5, is that of an open orbit (i.e., the ultrasonic attenuation coefficient is a minimum at infinite magnetic field). A satisfactory fit of the data, as well as an explanation of the phase, is obtained if twice the momentum is taken to be a measure of the dimension shown in Fig. 4(b). If we use this interpretation, then the portion of the dog's bone path giving rise to the periodicity has the characteristic of open orbits in that the electron moves in the same direction at those portions of its trajectory which are parallel to the sound wave fronts. The assumption that this period gives a measure of the dimension indicated in Fig. 4(b) would be perfectly valid if the Fermi surface were a sphere with necks stuck on it; however, if the Fermi surface is somewhat distorted from sphericity near the [112] directions, the dimensions measured may not be in a central (111) plane, but in a plane somewhat above or below it. If we assume that the surface is nearly spherical near [112], then twice the measured momentum plus the neck radius should equal a Fermi surface radius in the central (111) plane. This same relation holds for the open orbit measurements; in Table IV we have listed P/P_F and $2P/P_F$ plus the neck radius as a function of magnetic field orientation. A plot of these data is given in Fig. 5.

$q \| [112]$

We prepared parallel (112) faces on the copper and gold samples even though the possibility of exciting a pure longitudinal wave which would travel perpendicular to the parallel faces was questionable. As a check, the velocity of the sound wave was determined by a room-temperature measurement of the time required for 20 round trips through the samples; this

TABLE IV. Extremal Fermi surface dimensions for various magnetic field orientations with **q** parallel to [111].

H orientation	P/P_F			$(2P/P_F)$+neck radius		
	Cu	Ag	Au	Cu	Ag	Au
Parallel to $[2\bar{1}\bar{1}]$	0.382±0.011	0.389±0.018	0.387±0.011	0.959±0.033	0.920±0.048	0.954±0.027
3° from $[2\bar{1}\bar{1}]$	0.384±0.011	0.388±0.018	0.402±0.011	0.962±0.033	0.917±0.048	0.984±0.027
6°	0.386±0.011	0.392±0.018	0.375±0.011	0.966±0.033	0.925±0.048	0.929±0.027
9°	0.393±0.011	0.394±0.018	0.379±0.011	0.980±0.033	0.930±0.048	0.938±0.027
12°	0.394±0.011	0.402±0.018	0.384±0.011	0.983±0.033	0.945±0.048	0.948±0.027
15°	0.395±0.011	0.398±0.018	0.388±0.011	0.984±0.033	0.936±0.048	0.956±0.027
18°	0.406±0.011	0.420±0.020	0.392±0.011	1.006±0.033	0.981±0.051	0.963±0.027
21°	0.423±0.012	0.424+0.020	0.406±0.011	1.040±0.035	0.989±0.051	0.992±0.027
24°	0.446±0.012	0.418±0.020	0.419±0.011	1.086±0.035	0.977±0.051	1.017±0.027
27°	0.439±0.012	0.440±0.020	0.416±0.011	1.072±0.035	1.021±0.051	1.012±0.027
30° from $[2\bar{1}\bar{1}]$ (parallel to $[1\bar{1}0]$)	0.426±0.012	0.470±0.021	0.400±0.011	1.045±0.035	1.082±0.054	0.979±0.027

value was corrected for density and elastic moduli changes, which would occur upon cooling to 4.2°K, and then compared with the theoretical value of a pure longitudinal wave at 4.2°K as calculated from accurate elastic-constants data.[13] The agreement was very good. As a further check, with **q**‖[112], belly orbits are observed with **H** along $[11\bar{1}]$ which give the Fermi surface radius along $[\bar{1}10]$; for both metals this value is in excellent agreement with the same Fermi surface dimension determined by the belly-orbit measurement with **q**‖[110]. In the same way, the neck radii determined from **q**‖[112] and **q**‖[110] data are in agreement (see Fig. 6). However, the shape of the neck from the hexagonal face to where it joins the main body of the Fermi surface is somewhat different. This is expected since the main body radius where the joining takes place varies. In Table V, we give the momentum values as a function of magnetic field orientation. For **H** near $[\bar{1}10]$, a dimension about two-thirds the size of a belly radius is found, and is interpreted as arising from a noncentral body orbit passing over two necks. For **H** between 25° and 60° from $[\bar{1}10]$, central belly periods are observed, and, for **H** between 60° and 90°, we find mixed belly and neck periods. This mixing causes little difficulty since the neck period persists at a much lower magnetic field and its period can be accurately determined by these low-field data alone; in addition, the difference in periods is so great that at the higher magnetic fields, the neck period shows itself only as a slowly varying

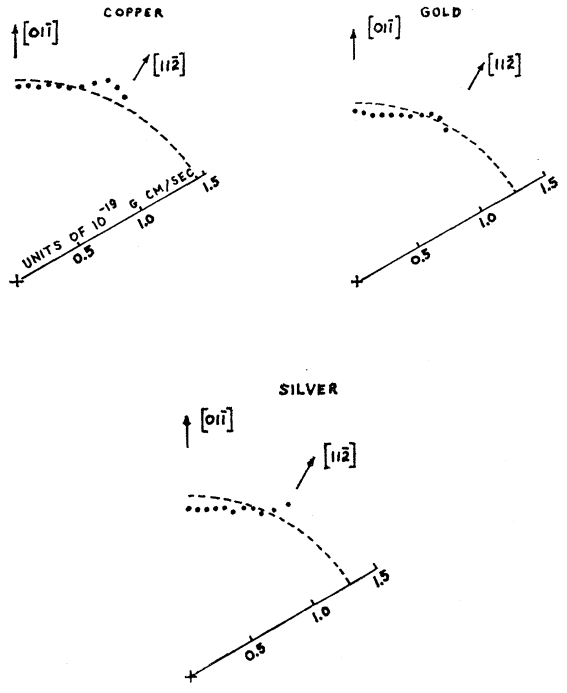

FIG. 5. Plot of experimental data in [111] Fermi surface cross section. These Fermi surface radii are given by $2P$ plus the neck radius, where P is the momentum corresponding to the observed periods. The dashed lines represent free-electron sphere radii.

[13] This information was kindly given to us by Dr. G. A. Alers of the Ford Scientific Laboratory.

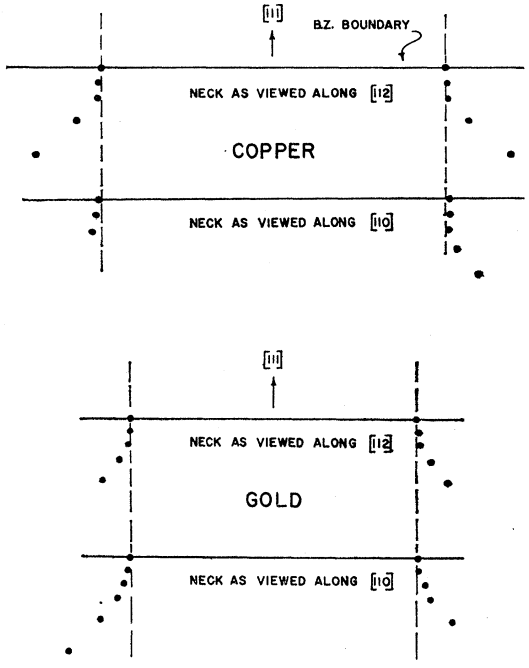

FIG. 6. Comparison of neck diameters in copper and gold as viewed along [110] and [112] directions.

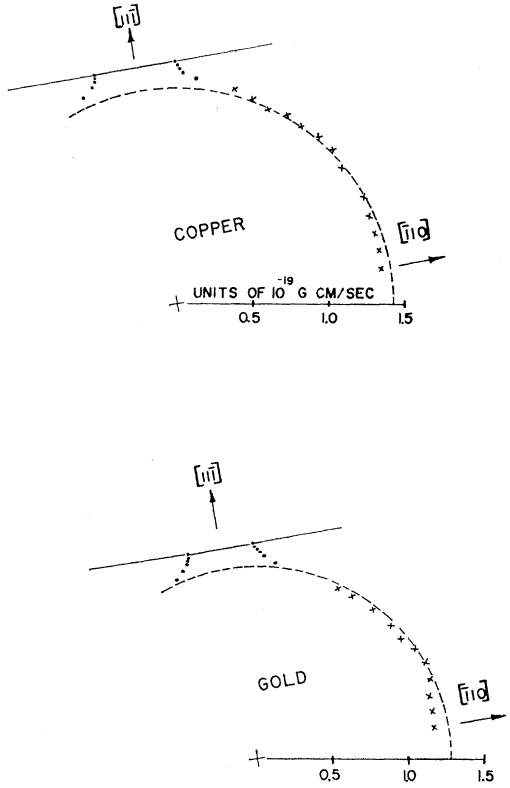

FIG. 7. Plot of experimental data in [112] cross section of the Fermi surface. The dots are neck-orbit measurements and the ×'s are belly-orbit measurements. The dashed lines represent free-electron spheres. Although the shape of both sides of the neck must be the same by symmetry, we have taken data on both sides and all of the plotted data represent independent measurements.

baseline for the belly oscillations. The Fermi surface in the (112) central plane is shown in Fig. 7.

Some shear wave measurements have been made in silver with **q** along [110] and the shear axis along [001] and [$\bar{1}$10], and were found to be in good agreement with those taken with longitudinal waves.

DISCUSSION

The probable errors given in the tables of data represent the accumulation of probable errors from: (a) the sound wave frequency measurement, (b) the calibration of magnetic field, and (c) the determination of the periods in $1/H$. That this error is representative of the uncertainty in the Fermi surface dimensions assumes, of course, that the relation between extremal $\hbar k$ and $\Delta(1/H)$ expressed in Eq. (1) is exactly correct.

The silver data presented here are in good agreement with the 230-Mc/sec data reported earlier[5] for the sound wave directions [110] and [100]. However, the present [111] data are considerably more accurate, partly due to the increase in frequency and partly because of the use of a sample of higher purity.

TABLE V. Extremal Fermi surface dimensions for various magnetic field orientations with **q** parallel to [112].

H orientation	P/P_F Cu	Au
Parallel to [$\bar{1}$10]	0.710±0.060	0.601±0.024
5° from [$\bar{1}\bar{1}$0]		0.588±0.024
10°	0.660±0.060	0.599±0.018
13°		0.623±0.018
25°	1.020±0.032	
30°	1.010±0.015	
35°	0.992±0.015	0.979±0.024
40°	1.010±0.021	0.980±0.024
45°	0.997±0.032	
47.5°		0.982±0.046
50°	1.012±0.032	
55°	1.010±0.021	0.974±0.036
60°	0.984±0.026	0.974±0.036
65°		0.997±0.036
		0.287±0.020
70°	0.994±0.042	1.013±0.024
	0.280±0.021	0.229±0.015
75°	0.974±0.053	0.985±0.012
	0.225±0.021	0.201±0.014
80°	0.961±0.011	0.949±0.012
	0.198±0.015	0.184±0.012
85°	0.963±0.011	0.941±0.012
	0.196±0.011	0.181±0.012
90° from [$\bar{1}$10] (parallel to [11$\bar{1}$])	0.956±0.011	0.930±0.012
	0.191±0.011	0.178±0.012

It should be pointed out that the argument used to explain why with **q**‖[111] the period giving the dimension indicated in Fig. 4(b) has the phase of an open orbit should apply equally well to the period giving the dimension A in Fig. 1 for **q**‖[110]. We have attempted to check this point, but the [110] data for this orientation show mixed periods both of which have rather small amplitude, and we have not been able to determine the phases with any degree of accuracy.

In Fig. 8, we show the [110] cross section for the Fermi surface of the noble metals and define various Fermi surface dimensions. In Table VI we give a comparison of our values of these dimensions with

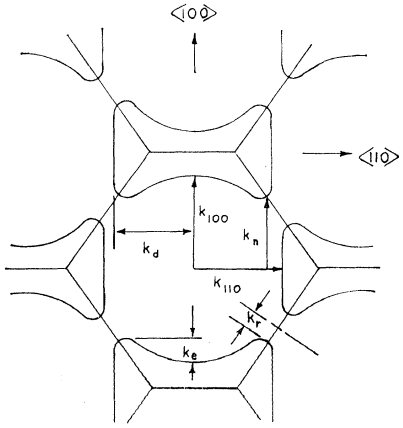

FIG. 8. The [110] cross section for the Fermi surface model defining various dimensions (after Burdick, see reference 17).

TABLE VI. Comparison of theoretical and experimental Fermi surface dimensions[a] as defined in Fig. 8.

Fermi surface dimension[b]	Bohm-Easterling (magnetoacoustic effect)[c] Cu	Ag	Au	Shoenberg (de Haas–van Alphen effect)[d] Cu	Ag	Au
$k_{100}(1)$	1.036±0.021		1.068±0.026			
(2)	1.100±0.060	1.072±0.065	1.127±0.071			
$k_{110}(1)$	0.957±0.011	0.933±0.012	0.941±0.012			
(2)	0.956±0.011	0.955±0.012	0.933±0.011			
(3)	0.959±0.032	0.920±0.048	0.954±0.027			
(4)	0.956±0.011		0.930±0.012			
k_d	0.852±0.009	0.876±0.011	0.868±0.011			
k_n	0.815±0.021	0.712±0.024	0.750±0.024			
k_e	0.284±0.042	0.360±0.045	0.377±0.045			
$k_r(1)$	0.195±0.011	0.142±0.012	0.180±0.006	0.200	0.137	0.177
(2)	0.191±0.011		0.178±0.012	0.200	0.137	0.177
k_{100}/k_{110}	1.11	1.13	1.17			

Fermi surface dimension[b]	Roaf[e] Cu	Ag	Au	Segall (band theory calculation)[f] Chodorow potential Cu	l-dependent potential Cu	Burdick (band theory calculation) Chodorow potential Cu	Morse *et al.* (magnetoacoustic effect)[g] Cu	Ag	Au
k_{100}	1.076	1.029	1.129	1.04±0.015	1.02±0.015	1.05±0.02	1.03	1.006	1.12
k_{110}	0.943	0.965	0.945	0.94±0.015	0.94±0.015	0.97±0.02	0.96	0.975	0.93
k_d				0.87±0.015	0.87±0.015	0.84±0.02			
k_n				0.76±0.015	0.81±0.015	0.77±0.015			
k_e				0.29±0.02	0.24±0.02	0.31±0.04			
$k_r(1)$				0.14±0.02	0.21±0.02	0.15±0.04	0.18		0.19
(2)	0.200	0.137	0.177			0.17±0.02			
k_{100}/k_{110}	1.14	1.07	1.20	1.10	1.09	1.09	1.07	1.03	1.20

[a] All dimensions are expressed in units of the free-electron Fermi sphere radii.
[b] (1) and (2) under k_r refer to the neck radius as measured along a line passing through the center of the hexagonal Brillouin zone face and the midpoint of one edge, and along a line passing through the center and one corner, respectively.
[c] (1) and (2) under k_{100} refer to the value found with q along [100] and [110], respectively. The four values of k_{110} refer to: (1) dog's bone measurement with q‖[100], (2) belly-orbit measurement with q‖[110], (3) open-orbit measurement with q‖[111], and (4) belly-orbit measurement with q‖[112].
[d] These neck radii are deduced from Shoenberg's data (reference 18) assuming circular necks.
[e] These dimensions were deduced by Roaf (reference 19) from Shoenberg's *dHvA* data (reference 18), Pippard's (reference 20), and Morton's (reference 21) anomalous skin effect measurements.
[f] These k values were kindly sent to us by Dr. Segall (private communication) and are based on work reported in references 15 and 16.
[g] See reference 14.

those determined by: (1) Morse *et al.*,[14] (2) band theory calculations made independently by both Segall[15,16] and Burdick,[17] (3) de Haas–van Alphen effect measurements made by Shoenberg,[18] and (4) Roaf's[19] empirical dimensions deduced from Shoenberg's measurements and from Pippard's[20] (Cu) and Morton's[21] (Ag) anomalous skin-effect measurements. Theory and experiment give a Fermi surface for Cu which is pulled out in the [100] directions, contracted in the [110] directions, and makes contact with the hexagonal face of Brillouin zone in the [111] directions. For most dimensions there is quantitative agreement between theory and experiment, a notable exception being the neck radius. Burdick's calculations indicate that the neck may not be of circular cross section; the radius computed along a line passing through the center of the hexagonal face and one corner being approximately 5% greater than that along a line passing through the center and the midpoint of one edge. We have made measurements of the neck radius along these two directions in gold and copper by propagating sound along the [112] and [110] directions and the results (shown in Fig. 6) indicate identical radii. Also Shoenberg's de Haas–van Alphen data for copper and gold infer neck radii which are in excellent agreement with our measurements if circular neck cross sections are assumed. These arguments would seem to indicate that this is no anisotropy in the neck radius. We list three values for the k_{110} dimensions for silver, and four values for copper and gold, which represent independent measurements since it is possible to determine this dimension with sound propagated along each of the axes we have studied. In Ag there is a discrepancy between the value determined by the dog's bone measurement with q‖[100] and the belly-orbit measurements with q‖[110]. In accord with the possible explanation for this difference which we give in an earlier report,[5] we believe that the belly orbit gives the correct dimension.

We give two values for k_{100}; (1) is from the belly period with q‖[100] and (2) is the sum of dimensions A plus B (Fig. 1) found with q‖[110]. Dimension (1) is deduced from more accurate data than (2), but it

[14] The copper and gold data are from reference 4, and the silver data are from R. W. Morse (private communication).
[15] B. Segall, Phys. Rev. Letters **7**, 154 (1961).
[16] B. Segall, Phys. Rev. **125**, 109 (1962).
[17] G. A. Burdick, Phys. Rev. Letters **7**, 156 (1961).
[18] D. Shoenberg (to be published).
[19] D. J. Roaf (to be published).
[20] A. B. Pippard, Phil. Trans. Roy. Soc. **A250**, 325 (1957).
[21] V. M. Morton, thesis, University of Cambridge, 1960 (unpublished).

TABLE VII. Calculated values of electron mean free paths and collision relaxation times.

Sample	Orbit	l from semilog plot (in units of 10^{-3} cm)	n_t (number of observed oscillations)	ql	ql/n_t	$H_{\min}$ (in kilogauss)	m^*/m	$\tau_1=cm^*/eH_{\min}$ (units of 10^{-11} sec)	$\tau_2=lm^*/\hbar k$ (units of 10^{-11} sec)
Ag I (170 Mc/sec)	Belly $\mathbf{H}\parallel[100]$	5.6	3.5	15.5	4.4	1.80	0.63	1.9	2.5
Ag I (230 Mc/sec)	Belly $\mathbf{H}\parallel[100]$	5.5	5.5	20	3.6	1.45	0.63	2.5	2.5
Ag II (348 Mc/sec)	Belly $\mathbf{H}\parallel[100]$	4.3	6	23	3.8	2.00	0.63	1.8	1.9
Au I (332 Mc/sec)	Belly $\mathbf{H}\parallel[100]$	6.4	12.5	38.5	3.2	1.10	1.19	6.2	5.5
Cu I (343 Mc/sec)	Belly $\mathbf{H}\parallel[100]$	12.0	15	54	3.6	0.74	1.39	10.6	10.5
Au I (130 Mc/sec)	Dog's bone	5.0	5.5	14	2.7	0.99	0.99	5.7	4.4
Au I (347 Mc/sec)	Dog's bone	4.0	11	28	2.7	1.28	0.99	4.5	3.5
Au I (332 Mc/sec)	Neck orbit	3.7	5	22	4.5	0.49	0.44	5.1	6.5

appears that (2) agrees better with Shoenberg and Roaf. Since the de Haas–van Alphen effect, in principle, precisely measures the Fermi surface and the interpretation of our data has been the simplest one suggested theoretically, one must seriously consider the possibility discussed by Pippard[9] that the periodicity of the oscillations may be determined by portions of the Fermi surface which are not extremal but by regions where the deformation parameter is large.

It has been assumed by several investigators[22,23] including ourselves,[5] that the mean free path l of the electrons is given approximately by the relation

$$l\cong n\pi\lambda, \tag{2}$$

where n is the order of the last observable magnetoacoustic oscillation as one goes to low magnetic field, λ is the sound wavelength, and thus $n\pi\lambda$ is the circumference of the electron orbit corresponding to the nth oscillation (the orbit is taken to be circular and stationary). Now since $q=2\pi/\lambda$, we obtain $ql=2n\pi^2$, which implies the rather stringent requirement that a ql value of about 20 is required per magnetoacoustic oscillation. However, Kjeldaas and Holstein[8] have predicted theoretically the number of oscillations for various ql values. From their curves it appears that the ratio of ql to n is consistently about 4. This is not as stringent a requirement on ql and implies that the mean free path of the electron need not be as large as the circumference of the largest orbit giving an observable oscillation. As a possible explanation of this we have considered the following simple argument. If we take the electron collision damping factor to be $N(d)/N(0)=e^{-d/l}$, where $N(d)/N(0)$ is the fraction of electrons left unscattered after moving a distance d, and further assume that the pulse-height amplitude of the nth oscillation is proportional to the number of electrons left unscattered after moving a distance $n\pi\lambda$ (real space circumference of the corresponding electron orbit), then we have that the ratio of the pulse-height amplitude of the $(n+i)$th oscillation to that of the ith oscillation is

$$\frac{V(n+i)}{V(i)}=e^{-[d(n+i)-d(i)]/l}=e^{-d(n)/l},$$

where for circular orbits $d(n)=n\pi\lambda$. If this reasoning is correct, one should be able to observe oscillations corresponding to orbit circumferences considerably larger than l provided $V(i)$ is large.

We have made plots of $\log[V(n+i)/V(i)]$ vs $n\pi\lambda$ for several sets of oscillations, three of which are shown in Fig. 9. In each case, the exponential behavior is verified and if d/l is the correct exponent, we readily obtain l from the slopes. In Table VII we list the l values determined in this way for various extremal orbits, along with the corresponding values of ql, n_t (total number of oscillations observed), and the ratio ql/n_t. This ratio ranges from 2.7 to 4.5, which is in agreement with the predictions of Kjeldaas and Holstein.

For the dog's bone we have taken $d(n)=0.85\ n\pi\lambda$, the factor 0.85 being estimated from our experimental

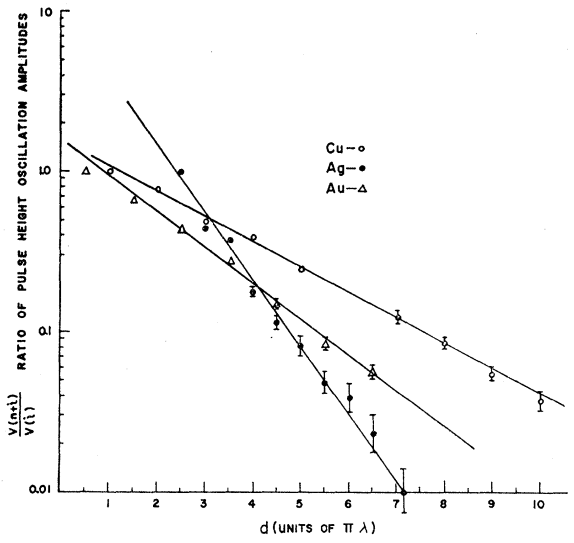

FIG. 9. Plot of the logarithm of the ratio of the pulse-height amplitude of the $(n+i)$th oscillation to that of the ith oscillation vs $n\pi\lambda$ for three central belly oscillations.

[22] J. A. Rayne and B. S. Chandrasekhar, Phys. Rev. **125**, 1952 (1962).
[23] B. W. Roberts, Phys. Rev. Letters **6**, 453 (1961).

plots of the Fermi surface shape. For the minimum neck orbit with **H** along [111], the group velocity of those electrons at the Brillouin zone boundary will be parallel to the boundary, and we have therefore taken the orbit to be essentially stationary such that $d(n)$ is given by $n\pi\lambda$.

It should be pointed out that according to the simple argument used above, the oscillations would be undamped for infinite mean free path, whereas theory[7] indicates that there will be damping even in the limit of extremely large ql. Thus, the plots in Fig. 9 give l values which are too small, the amount depending on the constant damping factor for the limit as ql becomes infinite.

Calculations of the electron relaxation time have been made in two ways: (1) A theoretical condition[7,8] for oscillations to occur is $\omega_c\tau>1$ where ω_c is the cyclotron frequency eH/cm^*, m^* being the effective mass. We expect therefore that this condition will break down, i.e., $\omega_c\tau\cong 1$ at the magnetic field value $H_{\min}$ where the last observable oscillation occurs and τ will be approximately given by $cm^*/eH_{\min}$. These values of τ are designated as τ_1 in Table VII where the corresponding values of $H_{\min}$ and m^*/m are also given.[24] (2) From the definition of $\tau=l/v$, where v is given by $\hbar\bar{k}/m^*$, $\bar{k}$ being the average k over the orbit ($\bar{k}\approx$perimeter$/2\pi$), we have obtained the values designated τ_2 in the table. The agreement between τ_1 and τ_2 is quite good, probably fortuitously so considering the number of approximations. The best agreement is found for the belly orbits, which is as expected since expressions for $d(n)$ and $\hbar\bar{k}$ are easily found using the fact that the orbits are stationary and approximately circular. On the other hand, $\hbar\bar{k}$ is rather uncertain for the dog's bone orbit and the form of $d(n)$ chosen for the neck assuming a stationary orbit may be questionable.

Cohen *et al.*[7] have calculated the theoretical qR positions ($qR=2\pi\hbar kc/\lambda eH$) of maxima and minima in the ultrasonic attenuation coefficient α, for the case $ql\gg 1$. We have compared these theoretical values with some typical experimental values. The comparison shows: (a) In agreement with our earlier paper on Ag,[5] the difference in qR between successive extrema in α is essentially constant for the experimental data, whereas the theory has the minima in α shifted towards high qR, (b) the experimental qR positions are found to remain the same, as one would hope, for the same orbit in the same metal observed at different frequencies, and (c) the phases of the oscillations vary depending on the metal and orbit being studied.

Lastly, it is necessary to point out that although the experimental error numbers we give for our work are realistic, there remain some 1–4% discrepancies among the numbers found by various investigators using different techniques. The origin of these discrepancies is not necessarily trivial. The theoretical foundation[7–10] of our data analysis includes a great many explicit and implicit assumptions, approximations, and conditions. To cite one example of an uncertainty: We do not know how wide the "strip of electrons" is that gives rise to magnetoacoustic oscillations or what $\Delta\hbar k$ constitutes the extremal region.

[24] The effective mass values for the various electron orbits in gold and silver are from Shoenberg (reference 18) and those for copper are from A. F. Kip, D. N. Langenberg, and T. W. Moore, Phys. Rev. **124**, 359 (1961).